Wave Functions for the F Center in Sodium Azide*†

Ralph H. Bartram and Pushpendra K. Jain
Physics Department and Institute of Materials Science, University of Connecticut, Storrs, Connecticut 06268

Peter J. Kemmey
Feltman Research Laboratories, Picatinny Arsenal, Dover, New Jersey

(Received 25 October 1972)

Wave functions have been calculated for the F center in sodium azide (NaN_3) in both the high-temperature (rhombohedral) and low-temperature (monoclinic) phases, by the point-ion method. The point symmetry at the anion site is D_{3d} in the rhombohedral phase and C_{2h} in the monoclinic phase. A predicted $A_1^+ \rightarrow E^-$ optical transition at 2.06 eV in D_{3d} symmetry corresponds to two transitions, $A^+ \rightarrow A^-$ at 1.82 eV and $A^+ \rightarrow B^-$ at 1.96 eV, in C_{2h} symmetry. The latter transitions are too close to resolve, and correlate well with the observed F band at 1.70 eV. An $A_1^+ \rightarrow A_2^-$ infrared transition at 0.82 eV in D_{3d} symmetry, which corresponds to an $A^+ \rightarrow B^-$ transition at 0.94 eV in C_{2h} symmetry, is polarized parallel to the hexagonal c axis, and could not be observed with the crystal orientations used in prior measurements. The calculated isotropic hyperfine interactions are larger by a factor of three than those inferred from ESR spectra, a common defect of point-ion calculations. However, it is shown that, as a consequence of wave-function anisotropy, the hyperfine constants remain nearly equal in spite of monoclinic distortion, thus explaining the resolved 19-line hyperfine pattern even in the monoclinic phase.

I. INTRODUCTION

Color centers in the alkali azides (NaN_3, KN_3, RbN_3, and CsN_3), which can be produced by ionizing radiation at low temperatures,[1-6] have been of interest for some time, since the corresponding defects are thought to be involved in photolysis and thermal decomposition at higher temperatures.[7,8] In the earlier studies,[1-3] purely speculative identifications of optical-absorption bands with F centers, V centers, and F-aggregate centers were made by analogy with the alkali halides. In particular the most prominent visible absorption in each case was attributed to the F center, one-electron trapped at an azide ion (N_3^-) vacancy. More recently the F center in uv-irradiated sodium azide (NaN_3) was detected at 90 °K by electron-spin resonance[9] and identified, apparently unambiguously, by its resolved 19-line hyperfine structure. Its ESR spectrum was subsequently correlated with an optical-absorption band at 730 nm,[5,6] rather than with the much more prominent absorption band at 610 nm; the latter was attributed instead to an F_2^+ center. Miller[6] has made a thorough study of the formation and bleaching of color centers in NaN_3. In particular he was able to produce the F band in isolation by a combination of heat treatment and illumination. It appears to be a single band about 0.4 eV wide, peaking at 730 nm, but with a long tail on the short-wavelength side extending to nearly 400 nm. The only theoretical treatment of color centers in alkali azides to date is a continuum-model calculation by King *et al.*[5] of F and F_2^+ centers. Their F-center calculation is not particularly illuminating, however, since it obscures the point symmetry of the defect and incorporates an effective dielectric constant adjusted to match the energy of the single predicted transition to that of the observed F band.

The crystal structure of NaN_3 was established by Hendricks and Pauling[10] in 1925 to be rhombohedral, with space group D_{3d}^5; the rhombohedral unit cell is shown in Fig. 1. More recently (1963), it was discovered by Miller and King, [11] and independently by Pringle and Noakes, [12] that NaN_3 undergoes a second-order phase transition at room temperature (~ 19 °C) and that the structure is monoclinic at lower temperatures. The nature of the distortion of the pseudorhombohedral unit cell is shown in Fig. 2. The monoclinic phase has been investigated in detail by Parsons and Yoffe,[13] and by Pringle and Noakes.[14] The latter authors designated the monoclinic phase α-NaN_3, and the rhombohedral phase β-NaN_3. The discovery of the phase transition was subsequent to the identification of the F center in NaN_3, and has contrary implications for that identification. It can be seen from Fig. 2 that the six Na^+ ions nearest the anion site are no longer equivalent in the monoclinic phase; rather, four of the Na^+ ions are closer to the anion site than are the other two. Consequently, one would no longer expect equal hyperfine interactions with all six cations, and the origin of the resolved 19-line hyperfine structure of the ESR spectrum at 90 °K is no longer evident.

The object of the present investigation is to determine whether the F-center model could account quantitatively for both the optical and ESR spectra, and in particular to resolve the dilemma posed by the 19-line hyperfine structure observed in the

monoclinic phase. To this end it is essential to adopt a fairly realistic model for the crystal potential, which includes details of the crystal structure and retains the true point symmetry of the defect. The point-ion potential model of Gourary and Adrian[15] is employed, but with much more flexible trial functions incorporating many variational parameters. Effects of extended ions and of lattice distortion and polarization have not been included.

Point-ion calculations for the F center in both rhombohedral and monoclinic NaN_3 are presented in Sec. II. Transition energies and transition moments are compared with the measured optical-absorption spectrum in Sec. III, and calculated spin-Hamiltonian parameters are compared with the experimental ESR spectrum in Sec. IV. The results are evaluated in Sec. V.

II. POINT-ION CALCULATIONS

The point-ion potential[15] can be justified as a model pseudopotential,[16] and the corresponding wave function as a pseudowave function from which the true wave function can be recovered by orthogonalization to ion-core orbitals. The point-ion potential can be expanded about the center of the anion vacancy in products of radial functions and linear combinations of spherical harmonics which transform as bases for the identity representation of the crystallographic point group at the anion site.

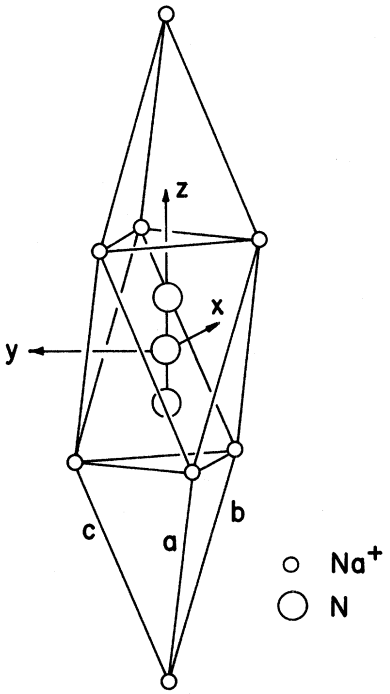

FIG. 1. Rhombohedral unit cell of β-NaN_3 (high-temperature phase).

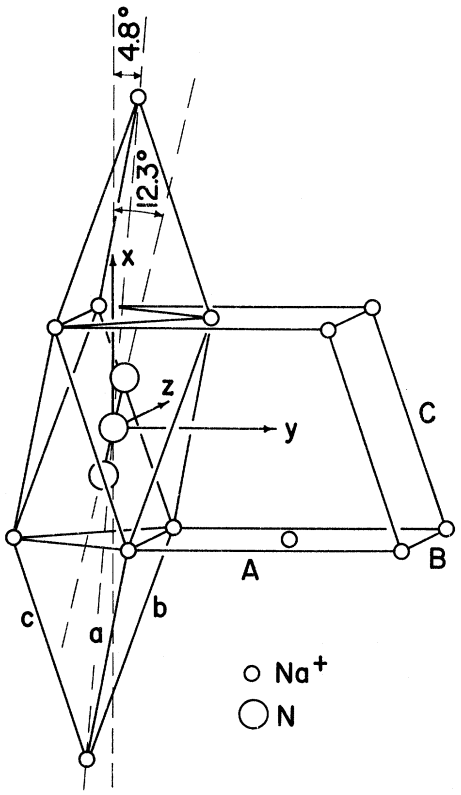

FIG. 2. Pseudorhombohedral unit cell of α-NaN_3 (low-temperature phase). Also shown are the cations associated with a conventional, base-centered-monoclinic unit cell.

This representation is an infinite sum, but if trial wave functions are expressed as linear combinations of functions which transform like spherical harmonics, only a finite subset of terms in the potential expansion makes a nonvanishing contribution to matrix elements of the potential. In their application of the point-ion approximation to F centers in alkali halides, Gourary and Adrian[15] chose simple s and p orbitals as trial functions. As a consequence of this restricted choice, only the spherically symmetrical part of the potential survived, since in O_h symmetry the next term in the potential expansion has $L = 4$. Many more terms must be retained in the present case because of both the relatively low symmetry and the flexible trial functions employed.

An additional complication arises in the application of the point-ion model to alkali azides. The azide ion itself has a substantial quadrupole moment, and so would be inadequately represented by a point charge. We chose to represent the azide ion by a linear array of three point ions, separated by 1.17 Å, with charges of $0.714e$ assigned to the central ion and $-0.857e$ assigned to each end ion.[17] A less convenient alternative would have been to

construct a multipole lattice.

The point-ion potential expansion can be expressed in the form (in Slater atomic units)

$$V_{p1}(\vec{r}) = -\sum_{L=0}^{\infty}\sum_{M=-L}^{L} Y_L^M(\theta,\phi) \times\left(e_{LM}r^L + \sum_{s<} f_{LMs}\frac{r_s^L}{r^{L+1}} - \frac{r^L}{r_s^{L+1}}\right) , \quad (1)$$

where

$$e_{LM} = \sum_{\alpha=0}^{\infty} \frac{8\pi Q_\alpha}{(2L+1)r_\alpha^{L+1}} Y_L^{M*}(\theta_\alpha,\phi_\alpha) \quad (2)$$

and

$$f_{LMs} = \sum_{\alpha, r_\alpha = r_s} \frac{8\pi Q_\alpha}{(2L+1)} Y_L^{M*}(\theta_\alpha,\phi_\alpha) . \quad (3)$$

Here, Q_α is the charge on ion α whose polar coordinates with respect to the vacancy center are r_α, θ_α, and ϕ_α, and $Y_L^M(\theta,\phi)$ is a spherical harmonic. The sum $\sum_{s<}$ in Eq. (1) is only over spherical shells of ions whose radius r_s is less than r. The sum in Eq. (3) is over ions on a single spherical shell. As noted above, only a finite set of terms in Eq. (1) needs to be evaluated. Each term in Eq. (1) is a solution of the Laplace equation, except at a shell of ions $r = r_s$, where the radial function suffers a discontinuous change in slope. The required terms in the potential expansion were evaluated out to 50 shells of ions; that is, within a spherical volume of radius $R = r_{50}$. The infinite-lattice sums in Eq. (2) were evaluated by the method of Nijboer and de Wette.[18,19]

Point-ion calculations for the F center in NaN_3 have been performed for both the rhombohedral and monoclinic phases, in order to display the effects of the monoclinic distortion on wave functions and energy levels. The description of the electronic structure is simpler in the rhombohedral phase, because of the higher site symmetry, so calculations for this phase will be presented first. However, it should be emphasized that the F center is never stable above room temperature, where this phase occurs.

A. Rhombohedral Phase

The rhombohedral unit cell is shown in Fig. 1. Its dimensions[20] are $a = 5.488$ Å and $\alpha = 38°43'$. The N nuclei are located at $(\frac{1}{2},\frac{1}{2},\frac{1}{2})$ and $\pm(u,u,u)$, where $u = 0.425$; the resulting N-N distance is 1.17 Å. The point symmetry at the azide site is D_{3d}. Coordinate axes were chosen as shown in Fig. 1, with the z axis coincident with the triad axis.

Trial functions were expressed as single-center expansions about the vacant azide site. Symmetry-adapted combinations of spherical harmonics up to $L = 3$ were combined with the following normalized radial functions to construct the basis functions listed in Appendix A:

$$R_0(r) = (\tfrac{4}{3}\zeta^3)^{1/2}(1+\zeta r)e^{-\zeta r} , \quad L = 0 ; \quad (4)$$

$$R_L(r) = [(2\zeta)^{2L+3}/(2L+2)!]^{1/2} r^L e^{-\zeta r} , \quad L > 0 . \quad (5)$$

The trial functions $\phi_n(\Gamma,\vec{r})$ are then related to the basis functions $\chi_m(\Gamma;\vec{r})$ by

$$\phi_n(\Gamma,\vec{r}) = \sum_m \chi_m(\Gamma;\vec{r}) C_{mn}(\Gamma) , \quad (6)$$

where Γ denotes the irreducible representation. The expansion coefficients $C_{mn}(\Gamma)$ and orbital exponents ζ_m were varied to minimize the ground-state energy. The calculated energies of low-lying states $E_n(\Gamma)$ are listed in Table I, and the optimum values of wave-function parameters in Table II.

B. Monoclinic Phase

The pseudorhombohedral unit cell for the monoclinic phase is shown in Fig. 2. Its relation to the conventional base-centered monoclinic unit cell is also illustrated in Fig. 2. The dimensions of the monoclinic cell were established by Pringle and Noakes[14] at a temperature between -90 and -100 °C; they are $A = 6.21$ Å, $B = 3.66$ Å, $C = 5.32$ Å, and $\beta = 108.4°$. The N nuclei are located at $(0, \frac{1}{2}, \frac{1}{2})$ and $(\pm 0.1016, \frac{1}{2}, \frac{1}{2} \pm 0.2258)$. The axes of the pseudorhombohedral cell are related to those of the monoclinic cell by

$$\vec{a} = \tfrac{1}{2}(\vec{A} - \vec{B}) + \vec{C} , \quad (7)$$

$$\vec{b} = \tfrac{1}{2}(\vec{A} + \vec{B}) + \vec{C} , \quad (8)$$

$$\vec{c} = \vec{C} . \quad (9)$$

From these relations, one obtains the following dimensions of the pseudorhombohedral cell: $a = b = 5.56$ Å, $c = 5.32$ Å, $\alpha = \beta = 38°38'$, $\gamma = 38°28'$, the N nuclei are at $(\frac{1}{2},\frac{1}{2},\frac{1}{2})$ and $\pm(v,v,w)$, where $v = 0.3984$ and $w = 0.4774$, and the N-N distance is still 1.17 Å. Thus it can be seen that the distortion is relatively small, and consists primarily in shearing the planes of cations through 4.8° and tilting the azide ion through 12.3°, as shown in Fig. 2. However, the phase transition is by no means complete at this temperature,[14] so one can expect a somewhat greater distortion at 90 °K, where the ESR measurements were made.

TABLE I. Calculated energies for low-lying states of the F center in β-NaN_3 (rhombohedral phase). The parameter Γ denotes irreducible representations of point group D_{3d}, and energies $E_n(\Gamma)$ are in rydbergs.

Γ	$E_1(\Gamma)$
A_1^+	-0.3760
A_2^-	-0.3154
E^+	-0.1864
E^-	-0.2242

TABLE II. Wave function parameters for low-lying states of the F center in β-NaN_3 (rhombohedral phase), defined by Eqs. (4)–(6) in the text. The index m refers to basis functions listed in Appendix A. Expansions coefficients $C_{mn}(\Gamma)$ are dimensionless, where Γ denotes irreducible representations of point group D_{3d}, and orbital exponents ζ_m are in reciprocal Bohr radii.

Γ	m	$C_{m1}(\Gamma)$	ζ_m
A_1^+	1	0.9490	0.45
	2	0.3154	0.59
A_2^-	1	0.9883	0.41
	2	0.0717	0.85
	3	0.1350	0.71
E^+	1	0.9835	0.62
	2	0.1807	0.71
E^-	1	0.9093	0.36
	2	0.4161	0.65
	3	0.0035	0.65

The point symmetry at the azide site is reduced to C_{2h} in the monoclinic phase, since only one of the three diad axes and the inversion symmetry survive. It is expedient to choose a new coordinate system as shown in Fig. 2, this time with the z axis coincident with the diad axis. Basis functions were again constructed by combining the radial functions of Eqs. (4) and (5) with symmetry-adapted combinations of spherical harmonics, and are listed in Appendix B. The calculated energies of low-lying states $E_n(\Gamma)$ are listed in Table III, and the optimum values of expansion coefficients $C_{mn}(\Gamma)$ and of orbital exponents ζ_m are listed in Table IV.

III. OPTICAL-ABSORPTION BANDS

The low-lying energy levels of the F center in NaN_3 are compared for the rhombohedral and monoclinic phases in Fig. 3. The A_2^- and E^- levels in D_{3d} symmetry, which go over to one A^- and two B^- levels in C_{2h} symmetry, correspond to the triply degenerate $2p$ level in the continuum model; in view of the very large splitting of this level by the anisotropic part of the crystal potential, it is clear that one cannot simply interpret the observed F band as a $1s \rightarrow 2p$ transition.[5] The allowed transitions are also indicated in Fig. 3. The observed F band at 730 nm (1.70 eV) is well accounted for by the $A_1^+ \rightarrow E^-$ transition at 2.06 eV in D_{3d} symmetry which goes over to the $A^+ \rightarrow A^-$ and $A^+ \rightarrow B^-$ transitions at 1.82 and 1.96 eV, respectively; the latter are too close to be resolved. In D_{3d} symmetry the $A_1^+ \rightarrow E^-$ transition is polarized perpendicular to the hexagonal c axis, while the $A_1^+ \rightarrow A_2^-$ transition at 0.82 eV is polarized parallel to the c axis. The NaN_3 crystals grow as thin hexagonal plates, and the reported optical-absorption measurements

TABLE III. Calculated energies for low-lying states of the F center in α-NaN_3 (monoclinic phase). The parameter Γ denotes irreducible representations of points group C_{2h}, and energies $E_n(\Gamma)$ are in rydbergs.

Γ	$E_1(\Gamma)$	$E_2(\Gamma)$
A^+	−0.3760	−0.1310
A^-	−0.2420	
B^+	−0.1757	
B^-	−0.3063	−0.2309

were made with light propagating parallel to the hexagonal c axis.[5,6] With this experimental arrangement the $A_1^+ \rightarrow A_2^-$ transition could not be observed. The situation is more complicated in the monoclinic phase, but the qualitative conclusions are the same. Transition moments $\langle \vec{r} \rangle \equiv (\phi_f, \vec{r}\phi_i)$ for the three allowed transitions were calculated from the wave functions given by Eq. (6), Table IV, and Appendix B, and are listed in Table V. Also listed are oscillator strengths appropriate to unpolarized light propagating perpendicular to the crystal face (parallel to x in Fig. 2), given in atomic units by

$$f = \tfrac{1}{2}\Delta E(\langle y \rangle^2 + \langle z \rangle^2) . \tag{10}$$

It can be seen that the oscillator strengths for the higher energy transitions are comparable and are two orders of magnitude larger than that for the $A^+ \rightarrow B^-$ transition at 0.94 eV. Thus although it is no longer strictly forbidden in the monoclinic

TABLE IV. Wave-function parameters for low-lying states of the F center in α-NaN_3 (monoclinic phase), defined by Eqs. (4)–(6) in the text. The index m refers to basis functions listed in Appendix B. Expansion coefficients $C_{mn}(\Gamma)$ are dimensionless, where Γ denotes irreducible representations of C_{2h}, and orbital exponents ζ_m are in reciprocal Bohr radii.

Γ	m	$C_{m1}(\Gamma)$	$C_{m2}(\Gamma)$	ζ_m
A^+	1	0.9427	0.0851	0.45
	2	−0.1787	0.3531	0.57
	3	0.2735	0.1628	0.57
	4	0.0671	−0.9174	0.60
A^-	1	0.8651		0.37
	2	−0.2594		0.66
	3	0.3942		0.84
	4	−0.1702		0.66
B^+	1	0.9973		0.46
	2	−0.0732		0.44
B^-	1	0.9861	0.1202	0.41
	2	0.1225	−0.8375	0.41
	3	−0.0300	0.2216	0.60
	4	−0.0851	0.1180	0.62
	5	+0.0585	0.2368	0.67
	6	+0.0322	−0.4063	0.65

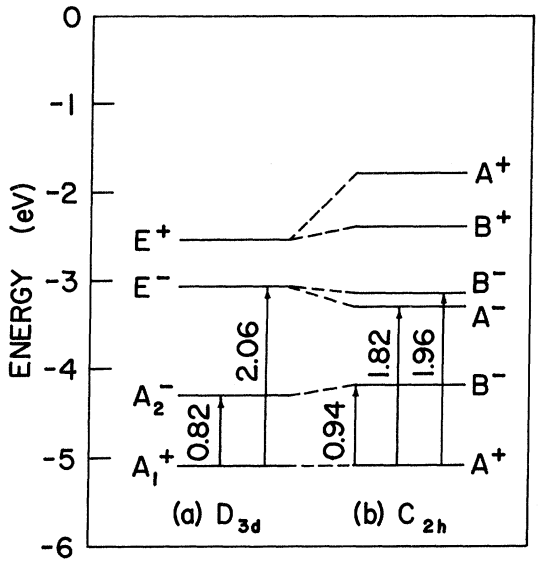

FIG. 3. Comparison of the low-lying energy levels of the F center in NaN_3 (a) in the rhombohedral phase and (b) in the monoclinic phase. The photon energies for allowed transitions are also indicated.

phase, one would not expect to observe the latter transition in the reported spectra; however, it should be very apparent in the absorption of light propagating perpendicular to the hexagonal c axis, a feasible measurement with sufficiently thick crystals.

IV. ELECTRON-SPIN-RESONANCE SPECTRUM

The ESR spectrum of the F center in NaN_3, reported by Carlson, King and Miller,[9] has a central g value of 2.003 ± 0.001, and has 19 resolved hyperfine lines separated by 9.1 ± 0.1 G. The nearly-free-electron g value is consistent with the F center model; the expected small negative g shift was not calculated.

The isotropic hyperfine interaction arises from the unpaired spin density at neighboring nuclei, and is given by $\sum_\gamma a_\gamma \vec{S} \cdot \vec{I}$, where

$$a_\gamma = \tfrac{16}{3}\pi (\mu_B \mu_I / I) |\psi_F(\vec{r}_\gamma)|^2 , \tag{11}$$

where $\psi_F(\vec{r}_\gamma)$ is the ground-state F-center wave function, obtained by orthogonalizing the ground-state envelope function $\phi_F(\vec{r})$ to the ion-core orbitals, evaluated at the nucleus of ion γ. With reference to Eq. (6), the function $\phi_F(\vec{r})$ is just $\phi_1(A_1^+, \vec{r})$ in D_{3d} symmetry and $\phi_1(A^+, \vec{r})$ in C_{2h} symmetry. We can express the orthogonalized wave function $\psi_F(\vec{r})$ by

$$\psi_F(\vec{r}) = N(1 - P)\phi_F(\vec{r}) , \tag{12}$$

where N is a normalization constant and P projects on occupied core orbitals,

$$P = \sum_\gamma \sum_c |\psi_{\gamma c}\rangle \langle \psi_{\gamma c}| . \tag{13}$$

If one neglects the variation of the envelope function over ion cores, i.e., one assumes

$$\langle \phi_F | \psi_{\gamma c} \rangle \approx \phi_F^*(\vec{r}_\gamma) \int \psi_{\gamma c}(\vec{r}) d\tau , \tag{14}$$

one obtains an approximate form for the hyperfine constant in terms of ϕ_F,[21]

$$a_\gamma = \tfrac{16}{3}\pi (\mu_B \mu_I / I) N^2 A_\gamma |\phi_\gamma(\vec{r}_\gamma)|^2 . \tag{15}$$

Here, A_γ is an amplification factor given by

$$A_\gamma = 1 - 2\sum_c \psi_{\gamma c}(\vec{r}_\gamma) \int \psi_{\gamma c}(\vec{r}') d\tau' + \sum_c \sum_{c'} \psi_{\gamma c}(\vec{r}_\gamma)\psi_{\gamma c'}(\vec{r}_\gamma) \times \int \psi_{\gamma c}(\vec{r}') d\tau' \int \psi_{\gamma c'}(\vec{r}'') d\tau'' . \tag{16}$$

The amplification factor for Na^+ was evaluated with analytic wave functions due to Clementi,[22] and has the value $A = 176.4$. Hyperfine constants for the six Na^+ ions nearest to the F center in NaN_3 were evaluated from Eq. (15), with the further approximation $N^2 \approx 1$, and are listed in Table VI. These six Na^+ ions are equidistant from the center of the azide site in the rhombohedral phase, but it is evident from Fig. 2 that the monoclinic distortion displaces two of them further from the center than the other four. It is a consequence of the anisotropy of the ground-state wave function in C_{2h} symmetry, manifest in the substantial admixture of s and d orbitals, that the contact hyperfine interactions are still nearly equal on these two types of ions, with that for the more remote ions actually larger.

The calculated hyperfine constants are larger by a factor of 3 than the measured hyperfine constant

TABLE V. Transition energies and transition moments for the allowed transitions in C_{2h} symmetry, defined with reference to the coordinate axes shown in Fig. 2. Oscillator strengths for light propagating parallel to the x axis are also listed.

	$A^+ \rightarrow B^-$	$A^+ \rightarrow A^-$	$A^+ \rightarrow B^-$
ΔE (eV)	0.94	1.82	1.96
$\langle x \rangle$	3.903	0.0	0.246
$\langle y \rangle$	0.520	0.0	−2.405
$\langle z \rangle$	0.0	2.377	0.0
f	0.009	0.379	0.420

TABLE VI. Isotropic hyperfine constants $a_\gamma/g\mu_B$ for the six Na^+ ions nearest the F center in NaN_3. The number of ions of each type and their distance from the center of the vacancy are also listed.

Symmetry	Number	r (Å)	$a/g\mu_B$(g)
D_{3d}	6	3.29	27.4
C_{2h}	4	3.22	27.6
	2	3.39	29.7

9.1 G. This discrepancy is a common failing of point-ion calculations, which tend to overestimate the hyperfine interactions with near neighbors,[23] and may not be serious.

The near equality of hyperfine constants in the monoclinic phase would appear to explain the resolved hyperfine structure. To first order, the magnetic field required for resonance is given by

$$H = h\nu/g\mu_B - \sum_{\mu=1}^{4} (a_1/g\mu_B)M_{I\mu} - \sum_{\nu=1}^{2} (a_2/g\mu_B)M_{I\nu} , \tag{17}$$

where the $M_{I\gamma}$ can independently take on the values $\frac{3}{2}, \frac{1}{2}, -\frac{1}{2}$, and $-\frac{3}{2}$. In the rhombohedral phase, $a_1 = a_2 = a$, and Eq. (16) predicts lines with the intensity ratios 1 : 6 : 21 : 56 : 120 : 216 : 336 : 456 : 546 : 580 : 546 : 456 : 336 : 216 : 120 : 56 : 21 : 6 : 1. In the monoclinic phase, a_1 and a_2 are different and the pattern breaks up into $13 \times 7 = 91$ distinct lines. However, as a consequence of the near equality of a_1 and a_2, these lines occur in groups corresponding to each of the original 19 lines. The groups corresponding to the three central lines of the 19-line pattern are shown in Fig. 4. It is clear that the 19-line pattern should remain very well resolved in spite of the splitting due to monoclinic distortion. Failure to resolve the lines within each group is presumably attributable to broadening produced by hyperfine interactions with more remote ions.

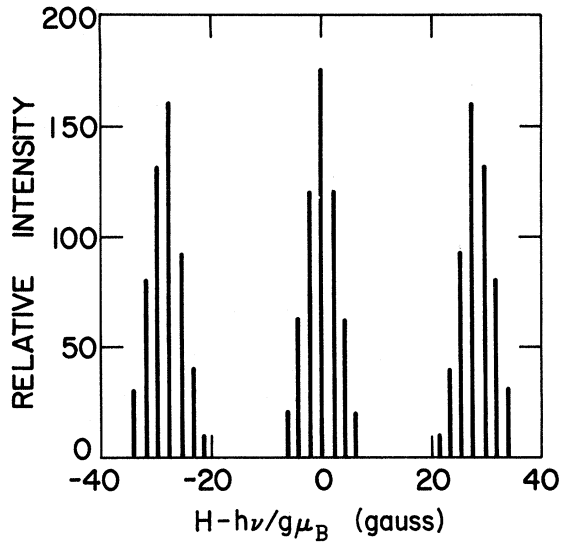

FIG. 4. Three central lines of the 19-line hyperfine structure, further split into components by the monoclinic distortion.

V. DISCUSSION

In summary, we have performed point-ion calculations for the F center in NaN_3 in both the rhombohedral and monoclinic phases. A predicted optical transition with two unresolved components corresponds well with the measured F band; these components have nearly perpendicular polarizations lying in the plane of the large crystal face, and it may be feasible to distinguish them with polarized light. An infrared band polarized perpendicular to the crystal face is also predicted and could be observed with a sufficiently thick crystal. The predicted hyperfine splitting of the ESR spectrum is exaggerated, a common failing of point-ion calculations. However, as a consequence of the anisotropy of the ground-state wave function, a resolved 19-line hyperfine pattern is predicted.

Thus the calculation was successful in resolving the dilemma of a 19-line hyperfine structure in the monoclinic phase, and the predicted optical transitions provide quantitative support for the F-center model, as well as suggestions for further observations.

The discrepancy in the magnitude of the hyperfine interaction is presumably attributable to the neglect of extended-ion effects[24,25]; present methods must be extended to include the molecular anion. Static distortion and polarization were also neglected,[26] as was the dynamic electron-lattice interaction, which determines the optical-absorption line shape[27]; these must await a detailed characterization of the sodium-azide lattice dynamics.

ACKNOWLEDGMENT

The authors are indebted to Professor O. R. Gilliam for helpful discussions.

APPENDIX A

Basis functions for the rhombohedral phase (β-NaN_3) are defined with respect to the coordinate axes shown in Fig. 1, and are classified according to the irreducible representations of point group D_{3d}. The following functions were constructed from s, p, d, and f orbitals, using the radial functions defined by Eqs. (4) and (5):

$$\chi_1(A_1^+; \vec{r}) = (\zeta^3/7\pi)^{1/2}(1+\zeta r)e^{-\zeta r} , \tag{A1}$$

$$\chi_2(A_1^+; \vec{r}) = (\zeta^7/18\pi)^{1/2}(2z^2 - x^2 - y^2)e^{-\zeta r} , \tag{A2}$$

$$\chi_1(A_1^-; \vec{r}) = (\zeta^9/72\pi)^{1/2}(x)(x^2 - 3y^2)e^{-\zeta r} , \tag{A3}$$

$$\chi_1(A_2^-; \vec{r}) = (\zeta^5/\pi)^{1/2}(z)e^{-\zeta r} , \tag{A4}$$

$$\chi_2(A_2^-; \vec{r}) = (\zeta^9/180\pi)^{1/2}(z)(5z^2 - 3r^2)e^{-\zeta r} , \tag{A5}$$

$$\chi_3(A_2^-; \vec{r}) = (\zeta^9/72\pi)^{1/2}(y)(3x^2 - y^2)e^{-\zeta r} , \tag{A6}$$

$$\chi_1(E^+; \vec{r}) = (2\zeta^7/3\pi)^{1/2}(yz)e^{-\zeta r} , \tag{A7}$$

$$\chi_2(E^+; \vec{r}) = (\zeta^7/6\pi)^{1/2}(x^2 - y^2)e^{-\zeta r} , \tag{A8}$$

$$\chi_1(E^-; \vec{r}) = (\zeta^5/\pi)^{1/2}(y)e^{-\zeta r} , \tag{A9}$$

$$\chi_2(E^-; \vec{r}) = (\zeta^9/120\pi)^{1/2}(y)(5z^2 - r^2)e^{-\zeta r} , \tag{A10}$$

$$\chi_3(E^-; \vec{r}) = (\zeta^9/12\pi)^{1/2}(z)(x^2 - y^2)e^{-\zeta r} . \tag{A11}$$

No basis function for the A_2^+ representation could be constructed from these orbitals; accordingly, it is presumed that a state of this symmetry would have too high a kinetic energy to be strongly bound. In the case of the two-dimensional E^+ and E^- representations, only functions belonging to the first row of each representation are listed.

APPENDIX B

Basis functions for the monoclinic phase (α-NaN_3) are defined with respect to the coordinate axes shown in Fig. 2, and are classified according to the irreducible representations of point group C_{2h}. The following functions were constructed from s, p, d, and f orbitals, using the radial functions defined by Eqs. (4) and (5):

$$\chi_1(A^+;\vec{r}) = (\zeta^3/7\pi)^{1/2}(1+\zeta r)e^{-\zeta r}, \quad \text{(B1)}$$

$$\chi_2(A^+;\vec{r}) = (\zeta^7/18\pi)^{1/2}(2z^2-x^2-y^2)e^{-\zeta r}, \quad \text{(B2)}$$

$$\chi_3(A^+;\vec{r}) = (\zeta^7/6\pi)^{1/2}(x^2-y^2)e^{-\zeta r}, \quad \text{(B3)}$$

$$\chi_4(A^+;\vec{r}) = (2\zeta^7/3\pi)^{1/2}(xy)e^{-\zeta r}, \quad \text{(B4)}$$

$$\chi_1(A^-;\vec{r}) = (\zeta^5/\pi)^{1/2}(z)e^{-\zeta r}, \quad \text{(B5)}$$

$$\chi_2(A^-;\vec{r}) = (\zeta^9/180\pi)^{1/2}(z)(5z^2-3r^2)e^{-\zeta r}, \quad \text{(B6)}$$

$$\chi_3(A^-;\vec{r}) = (\zeta^9/12\pi)^{1/2}(z)(x^2-y^2)e^{-\zeta r}, \quad \text{(B7)}$$

$$\chi_4(A^-;\vec{r}) = (\zeta^9/3\pi)^{1/2}(xyz)e^{-\zeta r}, \quad \text{(B8)}$$

$$\chi_1(B^+;\vec{r}) = (2\zeta^7/3\pi)^{1/2}(xz)e^{-\zeta r}, \quad \text{(B9)}$$

$$\chi_2(B^+;\vec{r}) = (2\zeta^7/3\pi)^{1/2}(yz)e^{-\zeta r}, \quad \text{(B10)}$$

$$\chi_1(B^-;\vec{r}) = (\zeta^5/\pi)^{1/2}(x)e^{-\zeta r}, \quad \text{(B11)}$$

$$\chi_2(B^-;\vec{r}) = (\zeta^5/\pi)^{1/2}(y)e^{-\zeta r}, \quad \text{(B12)}$$

$$\chi_3(B^-;\vec{r}) = (\zeta^9/120\pi)^{1/2}(x)(5z^2-r^2)e^{-\zeta r}, \quad \text{(B13)}$$

$$\chi_4(B^-;\vec{r}) = (\zeta^9/120\pi)^{1/2}(y)(5z^2-r^2)e^{-\zeta r}, \quad \text{(B14)}$$

$$\chi_5(B^-;\vec{r}) = (\zeta^9/72\pi)^{1/2}(x)(x^2-3y^2)e^{-\zeta r}, \quad \text{(B15)}$$

$$\chi_6(B^-;\vec{r}) = (\zeta^9/72\pi)^{1/2}(y)(3x^2-y^2)e^{-\zeta r}. \quad \text{(B16)}$$

*Supported by the U. S. Army Research Office-Durham under Grant No. DA-ARO-D-31-124-71-G35.

†The computational part of this work was performed at the Computer Center of the University of Connecticut, which is supported in part by National Science Foundation Grant No. GJ-9.

[1]F. C. Tompkins and D. A. Young, Proc. R. Soc. Lond. **A236,** 10 (1956).

[2]J. Cunningham and F. C. Tompkins, Proc. R. Soc. Lond. **A251,** 27 (1959).

[3]H. G. Heal and J. P. S. Pringle, J. Phys. Chem. Solids **15,** 261 (1960).

[4]H. A. Papazian, J. Phys. Chem. Solids **21,** 81 (1961).

[5]G. J. King, B. S. Miller, F. F. Carlson, and R. C. McMillan, J. Chem. Phys. **35,** 1442 (1961).

[6]B. S. Miller, J. Chem. Phys. **40,** 2371 (1964).

[7]P. W. M. Jacobs and F. C. Tompkins, Proc. R. Soc. Lond. **A215,** 265 (1952).

[8]J. G. Dodd, J. Chem. Phys. **35,** 1815 (1961).

[9]F. F. Carlson, C. J. King, and B. S. Miller, J. Chem. Phys. **33,** 1266 (1960).

[10]S. B. Hendricks and L. Pauling, J. Am. Chem. Soc. **47,** 2904 (1925).

[11]B. S. Miller and G. J. King, J. Chem. Phys. **39,** 2779 (1963).

[12]G. E. Pringle and D. E. Noakes, Acta Crystallogr. **16,** A192 (1963).

[13]R. B. Parsons and A. D. Yoffe, Acta Crystallogr. **20,** 36 (1966).

[14]G. E. Pringle and D. E. Noakes, Acta Crystallogr. B **24,** 262 (1968).

[15]B. S. Gourary and F. J. Adrian, Phys. Rev. **105,** 1180 (1957).

[16]B. S. Gourary and A. E. Fein, J. Appl. Phys. Suppl. **33,** 331 (1962).

[17]I. D. Campbell and C. K. Coogan, J. Chem. Phys. **44,** 2075 (1966).

[18]B. R. A. Nijboer and F. W. de Wette, Physica (The Hague) **23,** 309 (1957).

[19]B. R. A. Nijboer and F. W. de Wette, Physica (The Hague) **24,** 1105 (1958).

[20]R. W. G. Wyckoff, *Crystal Structures*, 2nd ed. (Wiley, New York, 1964), Vol. 2, p. 294.

[21]B. S. Gourary and F. J. Adrian, in *Solid State Physics*, edited by F. Seitz and D. Turnbull (Academic, New York, 1960), Vol. X, pp. 127–247.

[22]E. Clementi, IBM J. Res. Dev. **9,** 2 (1965). Tables of atomic functions are available as a supplement to this article.

[23]W. C. Holton and H. Blum, Phys. Rev. **125,** 89 (1962).

[24]R. H. Bartram and A. M. Stoneham, Phys. Rev. **176,** 1014 (1968).

[25]U. Opik and R. F. Wood, Phys. Rev. **179,** 772 (1969).

[26]A. M. Stoneham and R. H. Bartram, Phys. Rev. B **2,** 3403 (1970).

[27]D. B. Fitchen, in *Physics of Color Centers*, edited by W. B. Fowler (Academic, New York, 1968), pp. 294–349.